The effect of compressive loading on the residual gas permeability of concrete

Md Jihad Miah, Hatem Kallel, Hélène Carré, Pierre Pimienta, Christian La Borderie

The Effect of Compressive Loading on the Residual Gas Permeability of Concrete

Md Jihad Miah[1*, 2, 3] Hatem Kallel[2], Hélène Carré[2], Pierre Pimienta[1] and Christian La Borderie[2],

[1]Université Paris Est, Centre Scientifique et Technique du Bâtiment, 84 Avenue Jean Jaurès, Champs sur Marne, 77447 Marne-la-Vallée cedex 2, France

[2]ISA BTP-SIAME, Université de Pau et des Pays de l'Adour, Allée du Parc Montaury, 64600 Anglet, France

[3]Department of Civil Engineering, University of Asia Pacific (UAP), Dhaka-1215, Bangladesh

e-mails: jihad.miah@cstb.fr, jihad.miah@uap-bd.edu, hatem.kallel@univ-pau.fr, helene.carre@univ-pau.fr, pierre.pimienta@cstb.fr, christian.laborderie@univ-pau.fr

Abstract: Concrete permeability is related to pore connectivity and measures the flow rate of gases and liquids through the concrete under a pressure gradient. Information about concrete permeability - both in ordinary environmental conditions and after the exposure to high temperature - is, therefore, badly needed to better understand fluid transport in concrete, with specific reference to high temperature. In fact, permeability influences concrete spalling in fire by favoring pore-pressure build-ups during the heating process. In this research project, two different procedures are adopted to carry out permeability tests on concrete specimens either unloaded or preloaded during the heating process. The results show that concrete permeability strongly depends on crack width and orientation, both are affected by the axial compression or radial confinement.

* Corresponding author: Md Jihad Miah
Email: jihad.miah@cstb.fr

Keywords: Concrete, Temperature, Permeability, Confining pressure, Uniaxial loading.

1 Introduction

Fire spalling of concrete is a complex phenomenon, which might occur due to pressure build-up in the pores and thermal and load-induced stresses (Zhukov [1], Khoury and Anderberg [2], Miah et al. [3]). Miah et al. [3] showed that the loaded concrete specimens (B40-II and B40-III) are more likely to spall than unloaded specimens, with increasing amounts of spalling for higher values of applied load (uniaxial and biaxial loads). Interestingly, it was found that the fire spalling behavior of concrete slabs in unloaded conditions (0 MPa) and under a very low biaxial load (0.5 MPa, parallel to the heated face of the slab) can present two different scenarios. In the first case, no spalling has been observed in the unloaded specimen. In the second one, a uniform erosion extended to the whole heated area has been observed, for an average spalling depth of 12 mm. These results demonstrated that very low biaxial compressive loading can influence the fire spalling behavior of concrete, even though 0.5 MPa stress is very small compared to the compressive strength of concrete (51 MPa at the day of the fire test). This higher spalling behavior could not be explained only by the higher stresses (induced by the higher external load) but also by the higher pore pressure induced by a lower damage state and permeability (Felicetti and Lo Monte [4] and Choinska et al. [5]). Felicetti and Lo Monte [4], by implementing on the same biaxial fire tests an innovative technique based on ultrasonic pulse-echo have shown that damage was significantly reduced when the slabs were loaded, even at a very low biaxial stress (e.g. 0.5 MPa). Limited biaxial loads then can affect in a non-negligible

way the thermally induced microcracking and then reduce concrete permeability at high temperature.

Choinska et al. [5] showed that the permeability of concrete during heating up to 150 °C under uniaxial compressive loading (stress levels lower than 80% of the peak stress) is smaller than the permeability measured after unloading. Lion et al. [6] reported that the apparent permeability, measured after cooling, was lower when confining pressure was increased from 4 to 28 MPa and this was more significant for the higher thermal load. Chen et al. [7] tested the gas permeability of heat-treated mortars at four different levels of confining stresses (5, 12, 15 and 25 MPa). The authors observed that the permeability of mortars heat-treated above 400 °C was sensitive to confining pressure and the intrinsic permeability decreased by up to 23% when the confining stress increased from 5 to 25 MPa. Pei et al. [8] carried out longitudinal permeability and porosity tests on normalized mortar under different levels of confining pressure (5, 10, 20, 30 and 40 MPa). Their results showed that permeability decreases with the increase of confining pressure and shows a greater sensitivity to confining pressure at higher temperatures due to the closure of the cracks.

In order to gain a deeper understanding of the role of heating and loading on the permeability of concrete and to provide more insight into the mechanism behind the fire spalling of concrete, two ordinary concretes were tested. Residual longitudinal and radial permeability tests were carried out in unloaded and loaded (i.e. confining pressure and uniaxial compressive load) conditions on specimens. For an in-depth knowledge of the relationship between permeability and fire spalling, the permeability tests were conducted on the same two concrete mixes (B40-II and B40-III: $f_{c28days} \approx 40$ MPa) that have been studied in Miah et al. [3]. A more detail fire behavior of these two concretes (B40-II and B40-III) such as fire spalling, thermal properties,

mechanical properties, porosity, water absorption capacity and permeability in unloaded condition were investigated in Miah [9], Mindeguia [10], Carré et al. [11] and Mindeguia et al. [12-14].

2 Experimental investigations

2.1 Materials and concrete mix design

Two ordinary concretes, B40-II and B40-III, made respectively, with CEM II (CEM II/A-LL 42.5 R CE CP2 NF) and CEM III (CEM III/A 42.5 N CE CP1 NF) cements (NF EN 197-1:2012 [15]) have been investigated. The same mix design was used for both concretes; the only difference is the cement type. The CEM II cement contains 85% of clinker, 12% of calcareous fillers and 3% of slag, while the CEM III cement contains 54% of clinker, 3% of calcareous fillers and 43% of slag. The compressive strength (f_c) and splitting tensile strength (f_t) of both concretes were conducted according to NF EN 12390-3:2012 [16] and NF EN 12390-6:2012 [17], respectively, on cylindrical samples (diameter = 150 mm and height = 300 mm) at the age of 28 and 90 days. Constituents and concrete properties at the fresh and hardened state are reported in Table 1.

Table 1. Concrete mixture proportions and properties of hardened concrete

B40 Concrete	Unity	B40-II	B40-III
CEM II/A-LL 42.5 R CE CP2 NF (C)	kg/m^3	350	
CEM III/A 42.5 N CE CP1 NF (C)	kg/m^3		350
Calcareous 8/12.5 gravel	kg/m^3	330	
Calcareous 12.5/20 gravel	kg/m^3	720	
0/2 siliceous sand	kg/m^3	845	
Water (W)	l/m^3	189	
Water / cement ratio (w/c)		0.54	
28 days compressive strength	MPa	41.1 (36.4 – 46.8)	41.0 (36.1 – 46.5)
90 days compressive strength	MPa	50.9 (49.0 – 52.3)	50.4 (47.8 – 55.3)
28 days tensile strength	MPa	3.9 (3.9 – 4.0)	3.8 (3.7 – 3.9)
90 days tensile strength	MPa	4.8 (4.1 – 5.5)	4.3 (4.0 – 4.7)

2.2 Experimental programs, apparatus, and test procedures

2.2.1 Experimental program

Three different gas permeability tests were carried out in SIAME and CSTB. Within the scope of the study, a total of 40 concrete disc specimens were tested and about 200 measurements were carried out, see Table 2.

Table 2. Summary of the experimental test program.

T [°C]	80	120	250	400	600	800
i) Axial permeability tests under radial confining pressure (P_c = 0.3, 0.6, 0.9 and 1.2 MPa) after unloaded preheating	2/2	2/2	2/2	2/2	2/2	2/2
ii) Axial permeability tests under P_c of 0.6 MPa after preheating under uniaxial loading (σ = 0, 0.5, 1.5, 3 and 5 MPa)	–	–	–	2/2	–	–
iii) Radial permeability tests under uniaxial loading (σ = 0.6, 0.9, 1.2, 2, 3, 5 and 10 MPa) after unloaded preheating	–	2/2	2/1	2/2	1/–	–

Note: X/Y denotes the number of tested specimens (X B40-II samples and Y B40-III samples).

2.2.2 Axial permeability tests under radial confining pressure after unloaded preheating

The residual axial gas permeability of concrete was measured on 150 mm diameter and 50 mm thickness concrete disc (Fig. 1 right) using a Cembureau constant pressure permeameter (Fig. 1 left) (Kollek [18]). The concrete discs were cut from cylindrical specimens of 150 mm diameter and 300 mm height using a diamond disc. Upper and lower discs were not used to avoid the edge effect which could influence the measurements of permeability. The curved side of the specimen was wrapped with aluminum foil tape to ensure a good seal and to prevent leakage of gas through the curved side of the specimen in order that the flow occurs uniaxially through the thickness of the specimen.

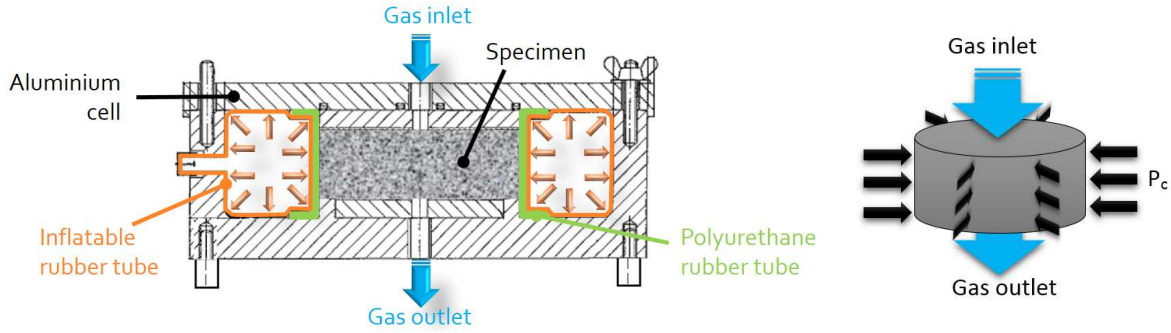

Fig. 1. Details of the permeability cell (left) (Kollek [18]) and confining pressure (P_c) and axial gas flow (right).

The permeability of concrete was investigated at room temperature after applying thermal loads of 120, 250, 400, 600 and 800 °C at a slow heating rate of 1 °C/min. The slow heating rate of 1 °C/min was chosen to limit undesirable thermal stress. After reaching the target temperature, the temperature was stabilized for 28, 10, 6, 6 and 6 hours, respectively, for the temperatures of 120, 250, 400, 600 and 800 °C (Hager [19]) to reach a uniform temperature in the concrete. The specimens were then cooled down to room temperature at a rate of lower than 1 °C/min inside the closed furnace. The reference specimens were dried in an oven at the temperature of 80 °C until a constant value of mass was reached (around 2 months) to evaluate water content.

To study the effect of confining pressure (perpendicular to the gas flow, Fig. 1 right) on the gas permeability of concretes (B40-II and 40-III), four different levels of radial confining pressure (P_c = 0.3, 0.6, 0.9 and 1.2 MPa, see Table 2) have been investigated. This was achieved by increasing the inflatable rubber tube pressure applied to the polyurethane rubber ring (Fig. 1 left). To ensure that the lowest applied load (0.3 MPa) is sufficient to prevent leakage of gas through the curved side, blank tests on an aluminum disc of the same dimensions (150 mm diameter and 50 mm thickness) were performed at 0.3 and 0.6 MPa. No outflow occurred at these lower confining pressures. Therefore, these blank tests demonstrated that the permeability test results of the

122 concrete specimens were not affected by leakage through the curved side even when applying the
123 lower load value.
124 Nitrogen has been chosen as the neutral percolating gas. Three levels of pressure difference
125 ΔP (the difference between the injection pressure P_{inj} and the atmospheric pressure P_{atm}) were
126 chosen depending on preheating temperatures in order to determine the intrinsic permeability of
127 concretes according to the Klinkenberg's approach (Klinkenberg [20]). Inlet pressures were
128 applied and maintained until gas flow stabilization.
129
130 2.2.3 Axial permeability tests under radial P_c of 0.6 MPa after preheating under uniaxial loading
131 The test method was similar to the test method described in previous section 2.2.2. The
132 difference was that the specimens were preheated under a constant uniaxial compressive loading
133 (Fig. 2). The size of the specimens was same as described in section 2.2.2. Only one heating
134 temperature (400 °C) was studied and the permeability tests were performed with one confining
135 pressure (P_c = 0.6 MPa). Prior to heating, all the specimens, as well as both concrete supports,
136 were ground in order to obtain two faces (upper and lower faces) parallel and plane to ensure a
137 uniform stress distribution in the specimens. Before heating, the specimens were wrapped by
138 means of a heating blanket (Fig. 2b) and a thermal insulator made with ceramic wool (Fig. 2c)
139 and was placed between both concrete supports in the compression testing machine. The
140 specimens were slowly heated (heating rate = 1 °C/min), stabilized for 8 hours, and then cooled
141 down to ambient temperature inside the heating device. The thermal insulator (i.e. ceramic wool)
142 ensure an appropriate increase of temperature during heating the specimens. Before heating, a
143 constant uniaxial compressive load was applied and then maintained constant during the heating
144 process, stabilization and cooling phases. Five different levels of uniaxial compressive stresses

145 (0, 0.5, 1.5, 3 and 5 MPa) have been investigated on both concretes (B40-II and B40-III), see
146 Table 2.

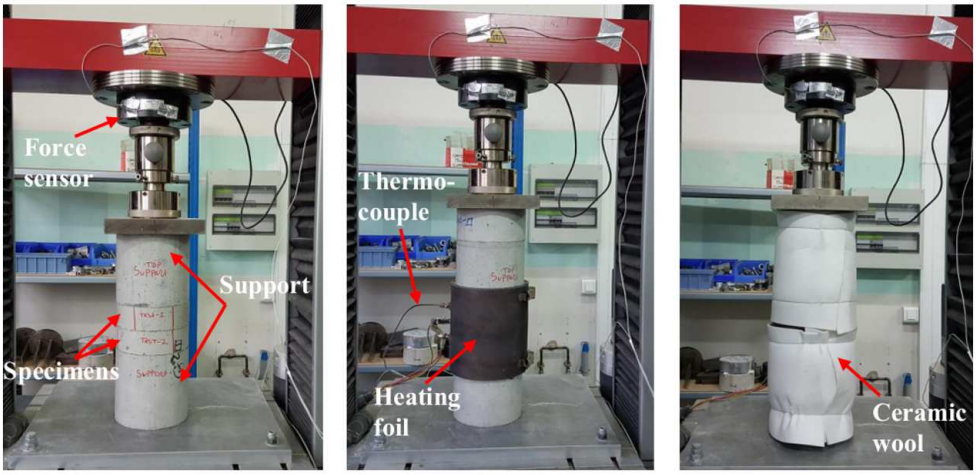

147 a b c

148 Fig. 2. Sample preparation before preheating under uniaxial loading of the test specimens (a.
149 specimen and concrete supports – b. specimen wrapped in the heating blanket – c. specimen with
150 insulating wool).

151 2.2.4 Radial permeability tests under uniaxial loading after heating without any applied preload

152 The principle of this test was to measure the radial permeability by injecting the nitrogen gas
153 inside a hollow concrete cylindrical disc and then measure the radial gas flow of the specimen
154 (Fig. 3). The hollow discs had external diameter, internal diameter and thickness equal to 123, 52
155 and 50 mm, respectively (Fig. 3 right). The concrete hollow discs were cut from cylindrical
156 specimens of 150 mm diameter and 300 mm height using a diamond blade and, as in the
157 previously described test, ground in order to obtain two faces (upper and lower faces) parallel
158 and plane to ensure a uniform stress distribution in the specimens. The specimens were drilled in
159 order to obtain 123 mm in outer diameter as well as to have better gas transfer, by avoiding the
160 edge effect, through the radial sides during the permeability test. The inner diameter is 52 mm

and the thickness 50 mm. The top and bottom faces of the specimens were sealed with aluminum foil tape to prevent leakage of gas along the interface (Fig. 3 right). The heating rate and the temperature levels were same as described in section 2.2.2.

In a similar way than the 2 methods described before, a constant relative pressure of the gas ΔP (the difference between the absolute injected pressure P_i and atmospheric pressure P_{atm}) is applied until the gas flow through the material is stabilized (permanent regime). The sample is placed in the permeameter cell between two metal plates (Fig. 3). The bottom plate is perforated in order to allow injecting the nitrogen at the bottom surface of the sample at a pressure P_i. The diameter of the plates is adapted for centering the cylindrical specimen. The nitrogen pressure is regulated by means of a controller and measured with the pressure sensor. In order to ensure a radial gas flow through the specimen, a circular rubber (Fig. 3 left) seals the connection between the specimen and the press plates. A minimal load (0.6 MPa) was applied on the specimen to maintain the good contact between the metal plates and the specimen faces by pressing the circular rubber joints.

In this device, the flow rate is measured upstream of the specimen by a mass flow meter, that converts a mass flow into a normalized volume flow. Flow and pressure measurements can be monitored in real time to control flow stabilization. In this testing setup, a time between 10 and 15 minutes is required for the gas flow to reach steady state conditions. Through flow measurement, the intrinsic permeability is determined by the Klinkenberg method (Klinkenberg [20].

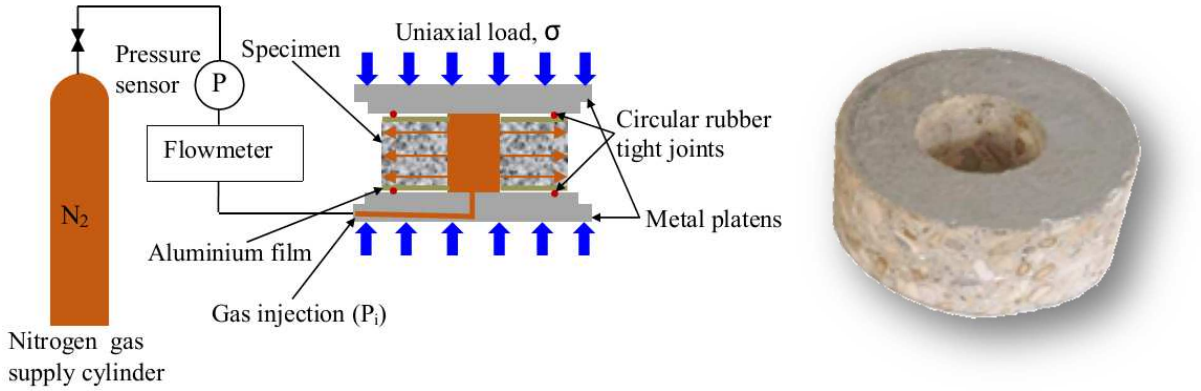

Fig. 3. Schematic diagram of the radial permeability test under uniaxial loading device left) and sample geometry (right).

The radial permeability measurements are carried out as part of a radial flow of the gas in steady state. The apparent permeability of a specimen is determined from Darcy's law applied to a laminar flow of a compressible fluid (gas). Thus, the apparent permeability K_a [m^2], based on a measurement of the upstream volumetric flow rate Q_i [m^3/s] at injection pressure Pi (Pa), is given by the following relationship (Choinska et al. [5]):

$$K_a = \frac{Q_i P_i \mu \ln\left(\frac{r_2}{r_1}\right)}{\pi h \left(P_i^2 - P_{atm}^2\right)} \quad (1)$$

where: μ [Pa.s] is the dynamic viscosity of the inlet gas used (nitrogen), P_{atm} [Pa] is the atmospheric pressure; r_1 [m], r_2 [m], h [m] are the inner radius, outer radius, and height of the cylindrical specimen respectively.

Before the test, a minimal compressive stress of 0.6 MPa was applied. This low load ensures the tightness of the permeability cell and then leads only to a radial gas flow. The value determined under the lower value of 0.6 MPa (equal to the preload compression stress) is assumed to be the reference permeability for this test. To study the effect of uniaxial compressive loading

195 on the radial gas permeability of concrete, seven different levels of compressive loading (0.6, 0.9,
196 1.2, 2, 3, 5 and 10 MPa, Table 2) have been investigated on both concretes.
197
198 **3 Experimental results and discussion**
199 3.1 Effect of radial confining pressure on the residual axial gas permeability of concrete
200 The residual axial intrinsic permeability (K_{int}) of concrete specimens subjected to different
201 preheating temperatures at different levels of radial confining pressure (P_c) is shown in Fig. 4a.
202 For an in-depth analysis of the influence of radial confining pressure on the axial permeability, it
203 is worthwhile to study the variation in permeability, normalized with respect to the reference
204 value of confining pressure, i.e. K_{int} (P_c)/K_{int} (P_c = 0.3 MPa) (Fig. 4b). In Fig. 4, the lines
205 represent the average value and the vertical line represents the range of data.

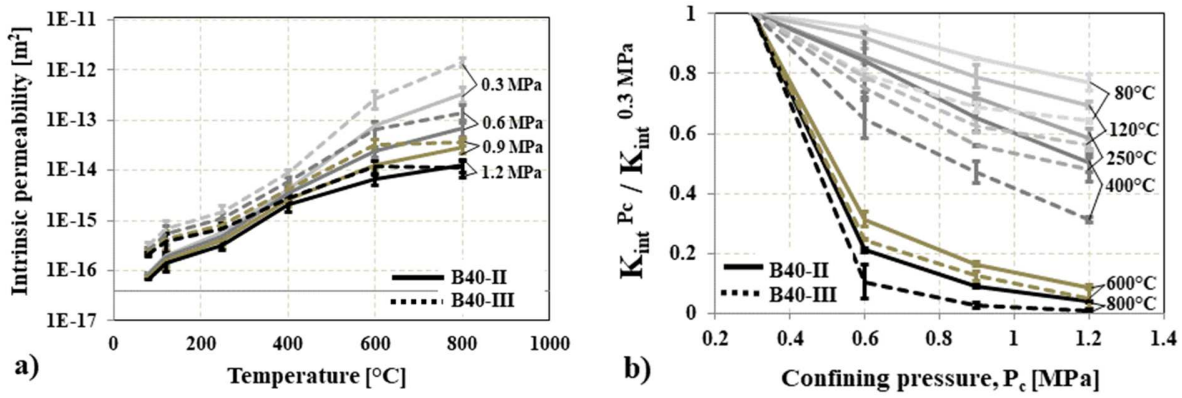

206 Fig. 4. Axial intrinsic permeability of concretes under different levels of confining pressure as a
207 function of temperature (a) and normalized permeability versus radial confining pressure (b).

208 In Fig. 4a, it can be seen that as the temperature increased, the permeability increased with
209 higher increments at the higher temperatures (note that the figure is in logarithmic scale for the
210 permeability). Between 80 °C and 120 °C, rather sharp increase of axial permeability was
211 observed for both concretes. This behavior was observed by Kalifa et al. [21] in the temperature

range between 80 °C and 105 °C. This behavior could be due to accessible pore volume caused by the removal of the free water and the physically bound water that was not withdrawn at 80 °C. Above 400 °C, the increase of the permeability may be attributed to the development of cracks mainly caused by the thermal incompatibility between the cement paste and the aggregates (Kalifa et al. [21]), since at high temperature the cement paste shrinks due to dehydration, while the aggregates dilate due to their thermal expansion. This mismatch induces tensile stresses in the matrix and compressive stresses in the aggregates which in turn can lead to cracks formation.

In Fig. 4b, the experimental results showed that the axial permeability of 2 concretes (B40-II and B40-III) decreased with increasing radial confining pressure (P_c perpendicular to the gas flow, Fig. 1 right). It can be seen that the residual permeability after preheating at 80 °C and 120 °C are hardly sensitive to confining pressure. This can be explained by the lower amount of microcracks and cracks induced by the lower preheating temperatures. On the contrary, these effects are more pronounced when the preheating temperatures are higher (e.g. at 600 °C and 800 °C). It is important to notice that, as previously mentioned, the decreased trend of permeability with increasing redial confining pressure is not due to leakage of gas, since no outflow occurred at confining pressure starting from 0.3 MPa during the blank test. This behavior should be attributed to the partial closure of heat induced microcracks and cracks (parallel to the gas flow) located at the aggregate-cement paste interface and through the aggregates. Indeed, the cracks perpendicular to the applied compressive stress (here stress due to confining pressure) close (Pei et al. [8]) while those parallel to the compressive stress tend to open (Mindeguia et al. [22], Huismann et al. [23] and Ring et al. [24]) (Fig. 5a and 5b). Fig. 5 is a schematic diagram showing the crack width changes with the effect of temperature and mechanical loading. Though, no measurement of crack openings were carried out on the tested samples, the

development of cracks presented in Fig. 5 is in good agreement with the permeability measurements and the results presented in Choinska et al. [5]. Crack width changes with temperature depend on concrete mixes and can be largely dependent on the nature of aggregates. As an example, crack widths of concretes containing flint aggregates are larger than most of other concretes when exposed to temperatures higher than 300 °C (Hager [19]). From the literature, it can be shown that the crack width of concretes heated at 300 °C and 400 °C can be about 3 µm (Huismann et al. [23]) and 10 µm (Kalifa et al. [21]), respectively. While Chen et al. [7] observed that the crack width of mortars heated at 400 °C can be about 2 to 5 µm.

Interestingly, a sharp decrease of permeability can be seen when the confining pressure was doubled (P_c = 0.6 MPa) than the reference pressure (P_c = 0.3 MPa). At the higher temperatures (600 °C and 800 °C), when the confining pressure continues to increase beyond 0.6 MPa, a lower decreasing rate of permeability is observed, and the permeability tends to stabilize. Fig. 4b suggests that, when temperatures are lower than 600°C, the crack closure and the decrease in permeability could continue if the confinement would have been increased beyond 1.2 MPa (which was the limitation of the test device). The presented results are in good agreement with the results reported in the literature even though most of the studies have been carried out at confining pressures that are much higher than in our tests (Lion et al. [6], Chen et al. [7] and Pei et al. [8]).

Fig. 4 allows us to compare the axial gas permeability of B40-II (3% of slag) and B40-III (43% of slag). It can be observed that the permeability of B40-III is higher for all the temperatures under 0.3 MPa confining pressure. The permeability difference between 2 concretes decreases when confining pressure increases.

Before permeability tests (i.e. during heating)	During permeability tests

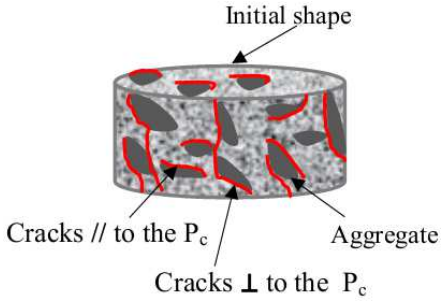

a) Multiple cracks due to thermal load

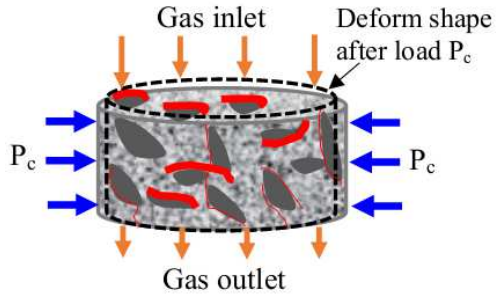

b) Width of cracks ⊥ to the P_c decreases and // to the P_c increases

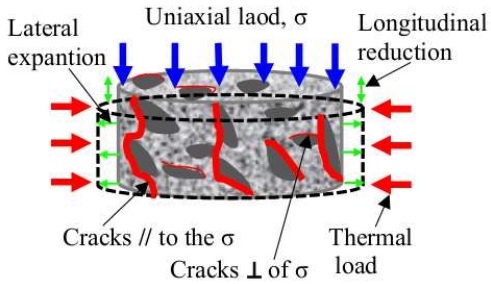

c) Width of cracks // to the uniaxial load (σ) increases and decreases ⊥ to the σ during heating-cooling

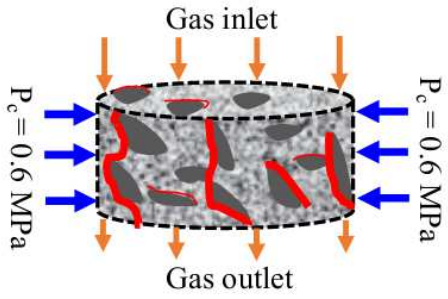

d) Axial gas flow (// to the vertical cracks) under confining pressure of 0.6 MPa

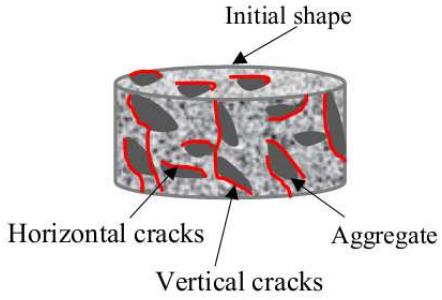

e) Multiple cracks due to thermal load

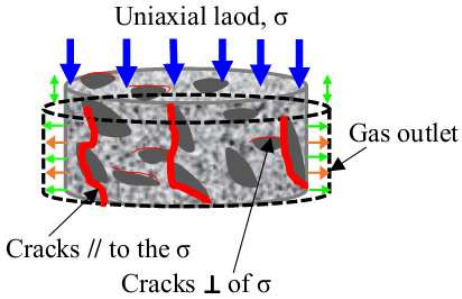

f) Width of cracks ⊥ to the load decreases

257 Fig. 5: Schematic diagram of the crack patterns and their effect on heating and different loading
258 conditions (Note: ⊥ = perpendicular, // = parallel).

259 3.2 The effect of uniaxial loading during heating-cooling on the axial gas permeability of concrete

260 The residual axial intrinsic permeability of the B40-II and B40-III concrete specimens
261 subjected to preheating (400 °C) under different levels of uniaxial compressive loading is
262 presented in Fig. 6a. In the diagram, the lines represent the average value and the vertical line

represents the range of data. In this experimental test campaign, an increasing trend of intrinsic axial gas permeability was observed with the increased uniaxial compressive loading (parallel to the gas flow) applied during the heating-cooling phases. Interestingly, a higher increase of intrinsic axial gas permeability was observed in the specimens which were loaded at low compressive loading (0.5 MPa). These results show that very small compressive loading can influence the axial gas permeability of concrete, even though 0.5 MPa stress is very small compared to the compressive (f_c) strength of concrete ($f_c \approx 50$ MPa at the day of the tests, see Table 1). It is to be noted that the heating of the specimens were carried out at 90 days. This age was chosen because at 28 days, the hydration of blended cements, as cements containing slags, is not completed and because 90 days is the advised age for laboratory tests in order to study a stabilized concrete with regard to its main properties (e.g. compressive strength).

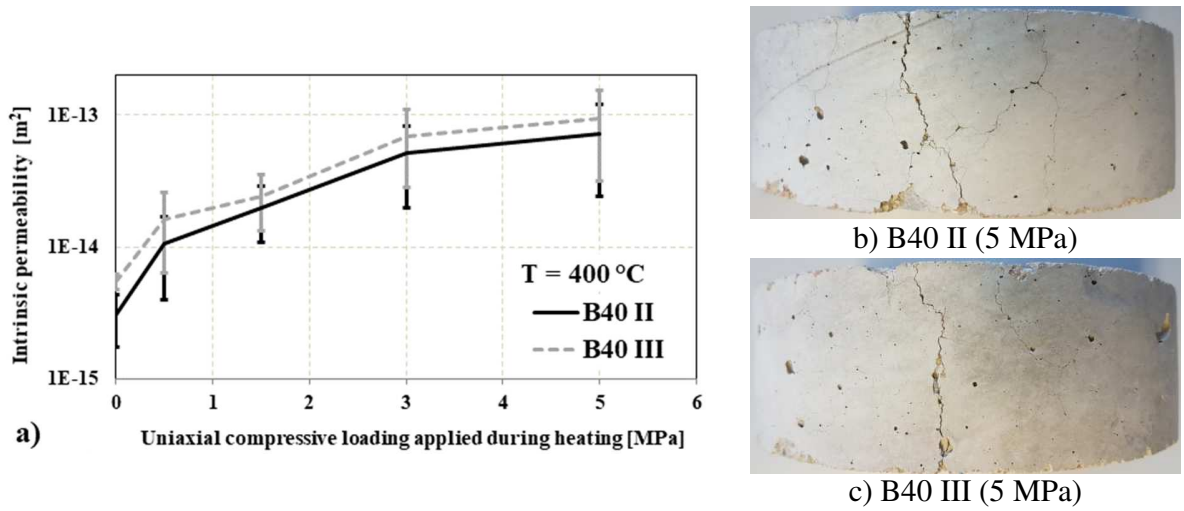

Fig. 6. Residual axial permeability measured after preheating under different levels of uniaxial compressive loading (a) and image of cracks parallel to the loading direction (σ = 5 MPa) (b-c).

When concrete is heated under a constant uniaxial compressive loading, its longitudinal strain is reduced. This reduction is mostly induced by transient thermal strain (Mindeguia et al. [22]).

By opposite, radial strains tend to be higher. This is mainly explained by the formation and opening of cracks parallel to the loading direction (Mindeguia et al. [22], Huismann et al. [23] and Ring et al. [24]) (see Fig. 5c). The evidence of cracks parallel to the loading direction after heat treatment at 400 °C under uniaxial loading (5 MPa) can be clearly seen in Fig. 6b and 6c. No similar cracking was observed in the unloaded specimens. These axial cracks explain the higher axial gas permeability measured in these tests, since the injected gas flow was along the compressive loading direction (Fig. 5d).

An important observation from Fig. 6a is that the residual axial permeability of B40-III (43% of slag) is higher than B40-II (3% of slag) in all the temperatures, which is in good agreement with the former tests that have presented in section 3.1 and Miah et al. [25].

3.3 The effect of uniaxial loading on the residual radial gas permeability of concrete

Fig. 7a presents the residual radial intrinsic permeability (K_{int}) of concretes (B40-II and B40-III) depending on uniaxial compressive stress. The relationships between the normalized permeability and the uniaxial compressive stress are shown in Fig. 7b. It can be seen that in Fig. 7b, at lower temperatures (120 °C and 250 °C), permeability decreases when applied compressive stress increases, while at higher temperatures (400 °C and 600 °C), the permeability decreases up to a certain level of load, after that stabilizes and then increases when the compressive stress increases.

In general, the trend presented in Fig. 7b clearly indicates distinct phases in the variation in radial permeability with the load. First, permeability decreased with the increasing applied compressive loading (for all temperature levels). This phenomenon is attributed to the partial closure of heat-induced microcracks and cracks (perpendicular to the load) caused by the increase in the applied compressive loading (Fig. 5f). It appears between 0.6 and 5 MPa for the

heating at 120 °C and 250 °C, between 0.6 and 2 MPa for 400 °C and between 0.6 and 0.9 for 600 °C.

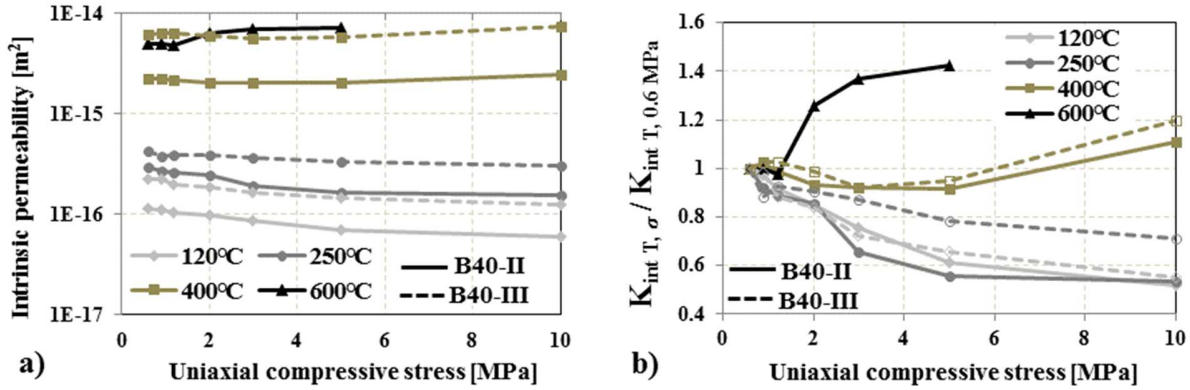

Fig. 7. Effect of uniaxial compressive loading on the radial gas permeability of concretes.

Secondly, a very small change or even almost constant permeability was observed. The observation in this phase can be explained by the counterbalancing of the cracks initiation and cracks growth by the cracks closure. This phase is observable up to 5 MPa for 120 °C and 250 °C, between 2 and 5 MPa for 400 °C and between 0.9 and 1.2 MPa for 600 °C.

Finally, an increase in permeability was observed with the further increase of the compressive stress. At 120 °C and 250 °C, the applied stress (10 MPa) is not sufficient to observe increase of permeability due to additional mechanical damage. For B40-II specimens heated at 400 and 600 °C, the phenomenon is observed above 5 and 1.2 MPa, respectively (Fig. 7b). Almost similar behavior was found for the B40-III preheated at 400 °C; The specimens preheated at 600 °C were more damaged during heating. Hence, it was not possible to measure the permeability due to the very fast gas flow.

The increasing permeability with increasing loads could be due to the extension of the existing cracks, creation, and opening of new cracks (Bian et al. [26]) due to Poisson's effect (i.e. increase transversal deformation due to crack opening in the direction of the gas flow).

As we have seen in sections 3.1-3.2 and in Miah et al. [25], B40-II (3% of slag) always exhibited lower permeability than B40-III (43% of slag) in all the heating levels (Fig. 7a). We then observe a good agreement among all the tests.

4 Concluding remarks

Permeability of concrete is one of the key parameters controlling internal fluid transfer; It influences the magnitude of pore pressure within the concrete structure which in turn contribute to the risk of fire spalling. It is worth noting, however, that the many studies have been conducted on the permeability of concrete at high temperatures under unloaded condition, while comparatively, there are few published data on the permeability of concrete subjected to heating and mechanical loading or under confining condition. To this end, axial and radial gas permeability tests were carried out on two ordinary concretes (B40-II and B40-III: $f_{c28days} \approx 40$ MPa) under different preheating and loading conditions. The permeability of concrete was investigated at room temperature after applying thermal loads of 80, 120, 250, 400, 600 and 800 °C at a slow heating rate of 1 °C/min.

The main findings regarding the influence of heating levels, loading type and levels, and cement type on the gas permeability of ordinary concrete can be summarized as follows:

I. As temperature increases, gas permeability increases as well, and the higher the temperature, the higher the increment.

II. The residual axial permeability of concretes (B40-II and B40-III) after unloaded preheating decreases with increasing radial confining pressure due to partial closure of heat induced axial microcracks and cracks (parallel to the gas flow) located at the aggregate-cement paste interface and through the aggregates.

342 III. Compressive loading affects concrete residual axial permeability even at low stress levels
343 (i.e. 0.6 MPa) compared with concrete strength ($f_c \approx 50$ MPa at the day of the tests) in
344 compression.
345 IV. When specimens are heated under a given preloading, the residual axial gas permeability
346 of concrete increases with the increasing uniaxial compressive loading (parallel to the gas
347 flow) applied during the heating-cooling phases. This behavior should be attributed to the
348 formation and opening of cracks parallel to the direction of the compressive loading
349 applied during preheating.
350 V. At lower temperatures (120 °C and 250 °C), the radial residual permeability under
351 uniaxial loading after heating without any applied preloading decreases with increasing
352 uniaxial compressive stress. While at higher temperatures (400 °C and 600 °C), the radial
353 permeability decreases up to a certain level of load, after that stabilizes, and then
354 increases when the uniaxial compressive stress increases. Such behavior may be
355 explained by the combination of two competing effects, crack closing due to compressive
356 stresses and crack opening due to the lateral expansion (Poisson's effect).
357 VI. Concrete permeability increases or decreases depending on the loading conditions and
358 becomes anisotropic. Hence, the stress state, by governing the orientation and opening of
359 the cracks is a key factor in controlling the transport of internal fluids (i.e. permeability)
360 and then directly triggers the build-up and magnitude of the pore pressure within the
361 concrete structure. Stress state has then 2 major roles on concrete fire spalling: (1) a
362 direct influence in the thermo-mechanical mechanism and (2) an indirect influence in
363 thermo-hydral mechanism by influencing the cracks opening and orientation and then, the
364 permeability.

VII. The permeability of B40-III (43% of slag) is higher than B40-II (3% slag) in all heating and loading conditions. Even if pore pressure is not the only driving force of spalling, these results (i.e. lower pore pressure due to higher permeability of B40-III at high temperatures) tends to show that the studied B40-III concrete could be less sensitive to fire spalling than B40-II concrete.

Acknowledgements:

This research was carried out in the frame of a large collaboration, on the influence of the mechanical loading on concrete spalling, between three laboratories: Politecnico di Milano, SIAME, and CSTB. Authors would like to thank Roberto Felicetti and Francesco Lo Monte of the Politecnico di Milano for the fruitful discussion.

Funding: This research did not receive any specific grant from funding agencies in the public, commercial, or not-for-profit sectors.

References:

[1] V.V. Zhukov, Reasons of explosive spalling of concrete by fire, Beton i zhlezobeton (Concrete and Reinforcement Concrete), Issue 3, 1976.

[2] G.A. Khoury, Y. Anderberg, Concrete spalling review, Fire safety design, report submitted to the Swedish National Road Administration, Sweden, 2000.

[3] M.J. Miah, F. Lo Monte, R. Felicetti, H. Carré, P. Pimienta, C. La Borderie, Fire Spalling Behaviour of Concrete: Role of mechanical loading (uniaxial and biaxial) and cement type, Key

Engineering Materials 2016, Vol. 711, pp. 549-555. DOI: 10.4028/www.scientific.net/KEM.711.549.

[4] R. Felicetti, F. Lo Monte, Pulse-echo monitoring of concrete damage and spalling during fire, Proceedings of the 9th International Conference on Structures in Fire, June 8-10, 2016, Princeton, USA.

[5] M. Choinska, A. Khelidj, G. Chatzigeorgiou, G. Pijaudier-Cabot, Effects and interactions of temperature and stress-level related damage on permeability of concrete, Cement and Concrete Research 37 (2007) 79–88.

[6] M. Lion, F. Skoczylas, Z. Lafhaj, M. Sersar, Experimental study on a mortar. Temperature effects on porosity and permeability. Residual properties or direct measurements under temperature, Cement and Concrete Research 35 (2005) 1937 – 1942.

[7] X-t. Chen, G. Caratini, C.A. Davy, D. Troadec, F. Skoczylas, Coupled transport and poro-mechanical properties of a heat-treated mortar under confinement, Cement and Concrete Research 49 (2013) 10–20.

[8] Y. Pei, F. Agostini, F. Skoczylas, The effects of high temperature heating on the gas permeability and porosity of a cementitious material, Cement and Concrete Research 95 (2017) 141–151.

[9] M.J. Miah, The effect of compressive loading and cement type on the fire spalling behaviour of concrete, PhD Thesis, 2017, Université de Pau et des Pays de l'Adour, France.

[10] J-C. Mindeguia, Contribution Expérimental a la Compréhension des risqué d'Instabilité Thermiques des Béton, PhD Thesis (French), 2009, Université de Pau et des Pays de l'Adour, France.

409 [11] H. Carré, C. Perlot, A. Daoud, M.J. Miah, B. Aidi, Durability of ordinary concrete after
410 heating at high temperature, Key Engineering Materials 2016, Vol. 711, pp. 428-435,
411 DOI: 10.4028/www.scientific.net/KEM.711.428.
412 [12] J-C. Mindeguia, P. Pimienta, H. Carré, C. La Borderie, On the influence of aggregate nature
413 on concrete behaviour at high temperatura, European Journal of Environmental and Civil
414 Engineering, Vol. 16, No. 2, February 2012, pp. 236–253.
415 [13] J-C. Mindeguia, P. Pimienta, H. Carré, C. La Borderie, Experimental analysis of concrete
416 spalling due to fire exposure, European Journal of Environmental and Civil Engineering, 2013,
417 Vol. 17, No. 6, pp. 453–466.
418 [14] J-C. Mindeguia, H. Carré, P. Pimienta, C. La Borderie, Experimental discussion on the
419 mechanisms behind the fire spalling of concrete, Fire and Materials, November 2015, Vol. 39,
420 Issue 7, pp. 619–635.
421 [15] NF EN 197-1, Cement - Part 1: Composition, specifications and conformity criteria for
422 common cements, April 2012.
423 [16] NF EN 12390-3: 2012, Testing hardened concrete - Part 3: Compressive strength of test
424 specimens, April 2012.
425 [17] NF EN 12390-6: 2012, Testing hardened concrete - Part 6: Tensile splitting strength of test
426 specimens, April 2012.
427 [18] J.J. Kollek, The determination of the permeability of concrete to oxygen by the cembureau
428 method - a recommendation, Materials and Structures (1989), 22, pp. 225-230.
429 [19] I.G. Hager, Comportement à haute température des bétons à haute performance-évolution
430 des principales propriétés mécaniques, PhD Thesis (French), 5 November 2004, l'Ecole
431 Nationale des Ponts et Chaussées etl'Ecole Polytechnique de Cracovie.

[20] L.J. Klinkenberg, The permeability of porous media to liquid and gases, American Petroleum Institute, Drilling and Production Practice (1941), pp. 200-213.

[21] P. Kalifa, G. Chéné, C. Gallé, High-temperature behaviour of HPC with polypropylene fibres: from spalling to microstructure, Cement and Concrete Research 31 (2001) 1487–1499

[22] J-C. Mindeguia, I. Hager, P. Pimienta, H. Carré, C. La Borderie, Parametrical study of transient thermal strain of ordinary and high performance concrete, Cement and Concrete Research 48 (2013) 40–52.

[23] S. Huismann, F. Weise, U. Schneider, Influence of the preload on the mechanical properties of high strength concrete at high temperatures, Proceedings of the 1st International Workshop on Concrete Spalling due to Fire Exposure, MFPA Institute, Leipzig, ISBN: 978-3-00-028604-9, September 3–5, 2009, pp. 189–200.

[24] T. Ring, M. Zeiml, R. Lackner, J. Eberhardsteiner, Experimental investigation of strain behaviour of heated cement paste and concrete, Strain (2013), 49, 249–256.

[25] M.J. Miah, P. Pimienta, H. Carré, N. Pinoteau, C. La Borderie, Fire spalling of concrete: effect of cement type, Proceedings of the 4th International Workshop on Concrete Spalling due to Fire Exposure, October 8-9, 2015, Leipzig, Germany.

[26] H. Bian, K. Hannawi, M. Takarli, L. Molez, W. Prince, Effects of thermal damage on physical properties and cracking behavior of ultrahigh-performance fiber-reinforced concrete, Journal of Materials Science, 2016, 51 (22), pp. 10066–10076.